Journal of the mechanical behavior of biomedical materials (xxxx) xxxx–xxxx

Contents lists available at ScienceDirect

Journal of the Mechanical Behavior of Biomedical Materials

journal homepage: www.elsevier.com/locate/jmbbm

3D-printing and mechanics of bio-inspired articulated and multi-material structures

Michael M. Porter[a,*], Nakul Ravikumar[a], Francois Barthelat[b], Roberto Martini[b]

[a] Department of Mechanical Engineering, Clemson University, Clemson, SC, USA
[b] Department of Mechanical Engineering, McGill University, Montreal, Quebec, Canada

ARTICLE INFO

Keywords:
Dermal armor
Fish scale
Shark skin
Boxfish carapace
Seahorse tail
Biomimetics

ABSTRACT

3D-printing technologies allow researchers to build simplified physical models of complex biological systems to more easily investigate their mechanics. In recent years, a number of 3D-printed structures inspired by the dermal armors of various fishes have been developed to study their multiple mechanical functionalities, including flexible protection, improved hydrodynamics, body support, or tail prehensility. Natural fish armors are generally classified according to their shape, material and structural properties as elasmoid scales, ganoid scales, placoid scales, carapace scutes, or bony plates. Each type of dermal armor forms distinct articulation patterns that facilitate different functional advantages. In this paper, we highlight recent studies that developed 3D-printed structures not only to inform the design and application of some articulated and multi-material structures, but also to explain the mechanics of the natural biological systems they mimic.

1. Introduction

The dermal armors of most living fishes are composed of relatively rigid elements, such as scales, denticles, scutes, or plates, embedded in a more compliant substrate, such as skin, which provide passive protection against predatory attacks (Chen et al., 2012; Song et al., 2011). Despite their relative stiffness, the complex articulations that join the individual protective elements often allow for considerable body mobility. Such integumentary joints are different from traditional skeletal joints (e.g., hinge, pivot, and ball-and-socket) (Levangie and Norkin, 2011); they typically form tessellating, overlapping, or interlocking connections (Ehrlich, 2015; Fratzl et al., 2016; Naleway et al., 2015; Sire et al., 2009; Vickaryous and Sire, 2009; Yang et al., 2013a). In fishes, these different connective mechanisms inherently provide varying degrees of combined puncture resistance and body flexibility (Gemballa and Bartsch, 2002; Long et al., 1996; Rudykh and Boyce, 2014a; Vernerey and Barthelat, 2010, 2014; Webb et al., 1992), as well as a suite of other vital functionalities, such as improved hydrodynamics and anti-biofouling (e.g., in sharks (Bechert et al., 1985; Bixler and Bhushan, 2012; Dean and Bhushan, 2010; Kesel and Liedert, 2007; Oeffner and Lauder, 2012; Raschi and Tabit, 1992)), body support (e.g., in boxfishes (Besseau and Bouligand, 1998; Yang et al., 2015)), and prehensility (e.g., in seahorses (Hale, 1996; Neutens et al., 2014; Porter et al., 2013; Praet et al., 2012)).

In addition to the multifunctional nature of most fish armors, the materials that make up these structures have also drawn considerable attention for their extraordinary mechanical properties. For instance, the scales of the *Arapaima gigas*, a fresh water fish of the Amazon Basin, can resist the penetrating bites of piranhas (Meyers et al., 2012); and, the scales of some teleosts have been shown to be amongst the toughest collagenous materials known (Dastjerdi and Barthelat, 2015). Similar to mammalian bone and abalone nacre (two of the most widely studied structural biological materials (Espinosa et al., 2009; Meyers et al., 2013; Wang and Gupta, 2011)), the toughness of most fish scales originates from their hierarchical structures composed of multiple layers of biomineral and biopolymer constituents (Barthelat and Mirkhalaf, 2013; Ritchie, 2011; Sen and Buehler, 2011; Studart et al., 2015). They also usually exhibit functional property gradients, often ranging from a harder exterior to a softer interior, which provides added resistance against impact, crushing, and piercing (Bruet et al., 2008; Torres et al., 2015; Yang et al., 2013b; Zhu et al., 2013).

Beyond the material-level (i.e., the nano-/micro-structural properties, and the topic of numerous reports (Allison et al., 2013; Bruet et al., 2008; Garrano et al., 2012; Gil-Duran et al., 2016; Ikoma et al., 2003; Lin et al., 2011; Porter et al., 2013; Raschi and Tabit, 1992; Torres et al., 2015; Yang et al., 2013b; Yang et al., 2015; Zhu et al., 2012; Zhu et al., 2013)), the shapes and articulation patterns of fish armors vary considerably among species (Ehrlich, 2015; Sire et al., 2009; Yang et al., 2013a), and often provide them distinct functionalities in addition to their primary purpose of protection. The armors of most

* Corresponding author.
E-mail address: mmporte@clemson.edu (M.M. Porter).

http://dx.doi.org/10.1016/j.jmbbm.2016.12.016
Received 23 June 2016; Received in revised form 16 December 2016; Accepted 20 December 2016

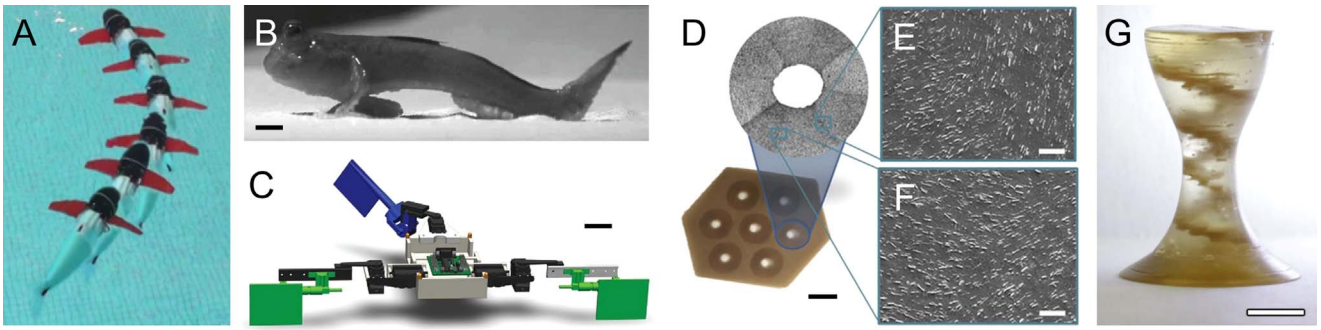

Fig. 1. Examples of some bioinspired robots (left) and materials (right) created by 3D-printing. **(A)** A robotic fish turning in a swimming pool and autonomously powered by hydraulic elastomer actuators in its tail, which were cast in 3D-printed molds. **(B)** A mudskipper (*Periophthalmus barbarous*) and **(C)** a 3D-printed robot (MuddyBot), which respectively serve as biological and robotic models used to study the locomotion transition from water to land in early tetrapods, such as *Ichthyostega*. **(D–F)** Micrographs of a 3D-printed, magnetically-aligned composite composed of magnetized ceramic platelets suspended in a polymeric matrix, which mimics the concentric osteonal microstructures of bone. **(G)** Image of a 3D-printed, magnetically-aligned structure with a helicoidal staircase formed from magnetized ceramic platelets suspended in a polymeric matrix, which mimics the microstructures of some common biological materials, such as the helical patterns in fish scales. Scale bars: (A) dimensions of the robot are 0.45 m × 0.19 m × 0.13 m; (B) 1 cm; (C) 4 cm; (D) 5 mm; (E & F) 25 μm; (G) 5 mm. Images adapted from (A) (Katzschmann et al., 2016); (B & C) (McInroe et al., 2016); (D-F) (Martin et al., 2015); (G) (Kokkinis et al., 2015).

extant fishes can be classified according to their form and material composition into five general categories: elasmoid scales, ganoid scales, placoid scales, carapace scutes, and bony plates. The structural forms and articulation patterns of a few representative fish armors are described in more detail in Section 3 of this paper.

Recently, the functional performance and mechanics of many fish armors have been revealed through mechanical testing and computational modeling approaches (Bruet et al., 2008; Chen et al., 2012; Dastjerdi and Barthelat, 2015; Meyers et al., 2012; Song et al., 2011; Torres et al., 2015; Vernerey et al., 2014; Wang et al., 2009; Yang et al., 2013b, 2014; Zhu et al., 2013; Zimmermann et al., 2013). Whereas these direct methods provide much insight into the structure-function behaviors of the biological systems, they can be somewhat limiting or invasive. Biological systems are highly variable (they never grow exactly alike) and because of their restricted availability (many organisms are protected or difficult to obtain), studying them can be a tedious and sometimes impossible task. Thus, in lieu of such direct methods, recent works used idealized geometries (disks) and simplified materials (glass) to study the interactions between hard protective plates and soft substrates (Chintapalli et al., 2014; Martini and Barthelat, 2016). However, with the recent accessibility and widespread use of three-dimensional (3D) printing technologies, it is now possible to build more complex models as representative proxies of natural systems in order to study their mechanical behaviors in controlled laboratory environments (Gu et al., 2016; Mohammed, 2016; Studart, 2016). Such biomimetic models can be analyzed without the need for developing computationally-expensive models or destructive testing of the natural specimens. For example, researchers can create idealized (or hypothetical) replicas that mimic the natural morphologies of specific biological systems to examine particular biomechanical functions. With this approach, it is possible to isolate and measure the individual mechanical contributions different structural minutiae may have on the overall performance of the biomimetic models and, by analogy, the natural systems they mimic. Such cross-disciplinary studies can not only lead to new discoveries in biology, but also result in the development of more 'biologically-informed' technologies for potential human applications, such as fish-inspired robots (Lauder, 2015; Raj and Thakur, 2016) or body armors (Araya et al., 2013; Duro-Royo et al., 2015).

To describe the multiple functions of the armored systems observed in fishes, we review representative studies where 3D-printed analogues were developed to reveal how the different morphological features in each system serve different mechanical roles. Specifically, we highlight studies that focus on four different functionalities (in addition to their primary protective function), namely: the controlled flexibility of overlapped and interlocked scales as seen in many teleosts and ancient fishes, the hydrodynamic properties of shark skins and boxfish carapaces, the structural body support of scutes as seen in boxfishes, and the prehensility of armored tails in seahorses. Although there have been many recent studies that use 3D-printing or other synthetic routes to fabricate biomimetic systems (Barthelat, 2015; Bouville et al., 2014; Chintapalli et al., 2014; de Obaldia et al., 2015; Dimas et al., 2013; Funk et al., 2015; Gao et al., 2015; Grunenfelder et al., 2014; Gu et al., 2016; Kim et al., 2012; Le Ferrand et al., 2015; Li and Ortiz, 2015; Martini and Barthelat, 2016; Meng et al., 2016; Mirkhalaf et al., 2014; Mirzaeifar et al., 2015; Molotnikov et al., 2015; Qin et al., 2014; Studart, 2016; Valashani and Barthelat, 2015; Wegst et al., 2015), the objective of this article is to review recent studies that use 3D-printing techniques to investigate the biomechanics of armored fishes specifically. We also provide a brief overview of current trends in 3D-printing for biological research, and describe ways these simple methodologies can be applied to study the mechanics of other similar biological systems of interest.

2. 3D-printing for biological research

Over the past few years, 3D-printing has been used as a tool to answer complex biological questions, many studies of which are highlighted in Section 4 of this paper. Some other recent studies include those that used 3D-printed structures to investigate the effects of morphology on the mechanics of some teeth (Crofts and Summers, 2014) and shells (Germann et al., 2014; Tiwary et al., 2015). Also, fish-inspired robots have been used to explain the influence of tail movements on fish swimming (using a robot built from parts cast in 3D-printed molds; Fig. 1**A**) (Katzschmann et al., 2016) and on the evolutionary transition of vertebrates from water to land (using a robot built from 3D-printed components; Fig. 1**B-C**) (McInroe et al., 2016). In these and similar studies (Ijspeert, 2014; Wegst et al., 2015), biomimetic systems that emulate natural systems are designed as virtual models, then built into physical prototypes. The models are typically derived from 3D renderings of the biological structures by various computer-aided design (CAD) and visualization techniques, from optical and electron microscopy to 3D laser scanning and x-ray computed tomography. The prototypes are most often formed directly by 3D-printing or indirectly by casting liquid polymers into 3D-printed molds (or both). While each additive manufacturing method uses slightly different means to build parts from the bottom up, most either extrude, polymerize, melt or bind materials together layer by layer. In contrast, subtractive manufacturing methods, such as computer numerical control (CNC) machining, remove material from a bulk solid to form custom-designed parts.

To date, the more common (and commercially-available) printers make predominantly plastic parts, but some metals, ceramics, and

composites can also be printed. For more comprehensive reviews on the state-of-the-art of additive manufacturing technologies, including 3D-printing, refer to Wong and Hernandez (2012), Vaezi et al. (2013), Gao et al. (2015), and Huang et al. (2015). Improvements in layer resolution, build time and size, as well as the types of materials that can be printed and their respective pre/post-processing methods will allow for the rapid development of hierarchically structured parts composed of multiple materials with more high-performance properties. In turn, it will likely be possible to (nearly) replicate the complex structures observed in nature for a variety of applications in relatively short lead times. In biomedicine, for instance, the potential of 3D-printing is incredible; fully functional and customizable 3D-printed organs that can grow and self-repair could replace the need for costly transplants and sub-par prosthetics (Murphy and Atala, 2014; Schubert et al., 2013). Resolutions down to the nano-scale (< 1 μm), similar to the sizes of the 'building blocks' of many natural materials, are now possible (Bauer et al., 2016; Fischer and Wegener, 2011), and this will likely enhance the performance of such structures. Moreover, recent developments in 3D-printing coupled with the manipulation of magnetized ceramic colloids have yielded hierarchical composites that mimic the anisotropic microstructures of some natural bio-composites, such as the concentric osteons of mammalian bone (Fig. 1**D–F**) (Martin et al., 2015) and the helical patterns of some fish scales (Fig. 1**G**) (Kokkinis et al., 2015).

Nevertheless, 3D-printing technologies still have a ways to go. Most commercially-available multi-material printers combine different polymers at resolutions generally on the order of ~100 μm to create parts with variable properties and/or colors. At higher resolutions (< 100 μm), such transitions can only be achieved with a few select materials (e.g., photopolymers) having a limited range of properties (e.g., with strengths up to tens of MPa and Young's moduli up to a few GPa (Rankouhi et al., 2016; Wu et al., 2015)). Also, more time and energy is often required to build multi-material parts (generally taking several hours to build a single part), than those with lower resolutions or single-material compositions. Therefore, the majority of studies to date that utilize 3D-printed parts to explore hypotheses on the form and function of biological systems make several necessary simplifications. Most often the bioinspired systems are scaled up to more manageable sizes. They are typically built solely from polymeric materials that, rather than matching the properties of their natural counterparts (which are often ceramic-polymer composites with strengths up to thousands of MPa and Young's moduli up to hundreds of GPa (Wegst and Ashby, 2004)), mimic the property variations of such in terms of approximate stiffness or hardness ratios. Also, many bioinspired systems rely on other post-processing methods or machined parts, such as solution casting or metallic joinery, in conjunction with the use of 3D-printed parts or molds to mimic the functional nuances of selected biological systems. In research, such simplifications are often convenient, not only for the fabrication of biomimetic systems, but also to elucidate their complex mechanics. To illustrate this, we review several examples of articulated and multi-material structures in the following sections inspired by the dermal armors of some living fishes and formed by 3D-printing or similar rapid prototyping techniques.

3. Classification of dermal armors in fishes

The dermal armors of living fishes can be classified according to their material composition, structural form and articulation patterns. Here we present a short description for each of the five types of fish armors shown in Fig. 2. They are categorized according to their material and structural organization as: (**A**) elasmoid scales, (**B**) ganoid scales, (**C**) placoid scales, (**D**) carapace scutes, and (**E**) bony plates. Here we make a distinction between the usually combined categories of 'carapace scutes' and 'bony plates' according to their respective structural forms and articulation patterns (tessellating vs. interlocking/overlapping). More comprehensive details on the classification of natural dermal armors and the scales of fishes, including some extinct forms (e.g., cosmoid and thelodont), are discussed in Vickaryous and Sire (2009), Sire et al. (2009), Yang et al. (2013a), and Ehrlich (2015).

3.1. Elasmoid scales

Elasmoid scales are the most common type of scales amongst extant fishes. They are imbricated, thin lamellar-like structures that protect a large majority of modern teleosts (Fig. 2**A**) (Ehrlich, 2015; Sire et al., 2009). The individual scales are composed of a basal layer of collagen fibers arranged into a type of cross-ply laminate (commonly termed 'elasmodine' (Sire and Huysseune, 2003)), which is covered by a highly-mineralized external layer (Allison et al., 2013; Ikoma et al., 2003; Lin et al., 2011; Zhu et al., 2012; Zimmermann et al., 2013). Elasmoid scales can be categorized as either cycloid or ctenoid according to their outer morphologies. The different morphologies typically occur in different species, but can also be found in different anatomical locations along a single fish (Kuusipalo, 1998; Lippitsch, 1990; Reza et al., 2009). The trailing edges of cycloid scales are smooth, as seen in salmon, while ctenoid scales have rougher, tooth-like surfaces, as common in striped bass (Ehrlich, 2015; Sire et al., 2009; Yang et al., 2013a). The scales are usually attached to the dermis by collagen fibers and embedded in a small pocket composed of skin (Sire and Huysseune, 2003; Zylberberg and Meunier, 1981). This provides the overlapping scales some freedom to bend and rotate (Rudykh and Boyce, 2014a; Vernerey and Barthelat, 2014), facilitating enhanced body mobility for locomotion (e.g., undulatory swimming).

3.2. Ganoid scales

Ganoid scales are thicker, rhomboid-shaped structures that overlap and interlock with peg-and-socket connections (Fig. 2**B**) (Gemballa and Bartsch, 2002; Varshney et al., 2015). These scales have a harder composition than elasmoid scales, consisting of an osseous basal plate, isopedine, and dentine, covered by a characteristic outer layer of 'ganoine' (Bruet et al., 2008; Yang et al., 2013b). They are attached to the dermis by thick Sharpey's fibers (Gemballa and Bartsch, 2002; Sire and Huysseune, 2003). Whereas ganoid scales are more rigid, and they were likely replaced through evolution by the more flexible and lighter elasmoid scales (Sire, 1989), their unique interlocking mechanism still permits considerable flexibility in such heavily armored fishes as gar and bichir (Gemballa and Bartsch, 2002; Long et al., 1996; Varshney et al., 2015; Webb et al., 1992).

3.3. Placoid scales

Placoid scales are characteristic of cartilaginous fishes, including rays and sharks (Fletcher et al., 2014; Motta et al., 2012; Raschi and Tabit, 1992). They are commonly referred to as 'dermal denticles' because of their tooth-like appearance and composition (Fig. 2**C**), which consists of an outer layer of enameloid and an inner layer of dentine that surrounds a pulp cavity (Fletcher et al., 2014; Motta et al., 2012; Raschi and Tabit, 1992). These scales, perhaps better described as partially imbricated, tooth-like protrusions in the shape of tiny hydrofoils, are periodically anchored into the skin at their base by Sharpey's fibers (Fletcher et al., 2014; Motta et al., 2012; Raschi and Tabit, 1992). Dermal denticles are best known for their drag reduction (Bechert et al., 1985; Dean and Bhushan, 2010) and anti-biofouling (Bixler and Bhushan, 2012; Kesel and Liedert, 2007) properties because of their uniquely ribbed microstructures.

3.4. Carapace scutes

Carapace scutes are a distinct form of armor found in some

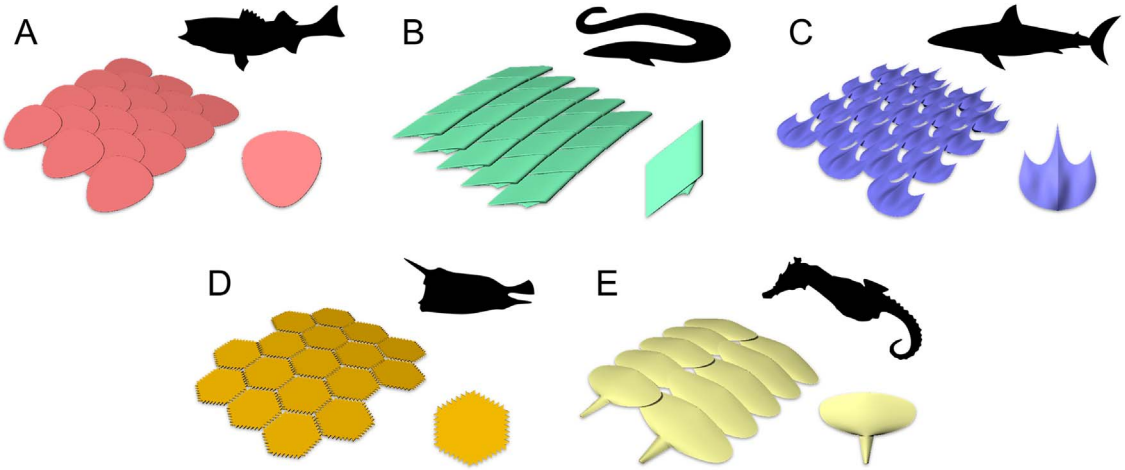

Fig. 2. Representative schematics of common protective armors among living fishes. **(A)** Overlapping elasmoid scales common among most teleosts, such as striped bass; **(B)** interlocking ganoid scales common among gars and bichirs; **(C)** partially imbricated placoid scales common among sharks; **(D)** tessellating carapace scutes common among boxfishes; **(E)** interlocking and overlapping bony plates common among seahorses and related syngnathid fishes.

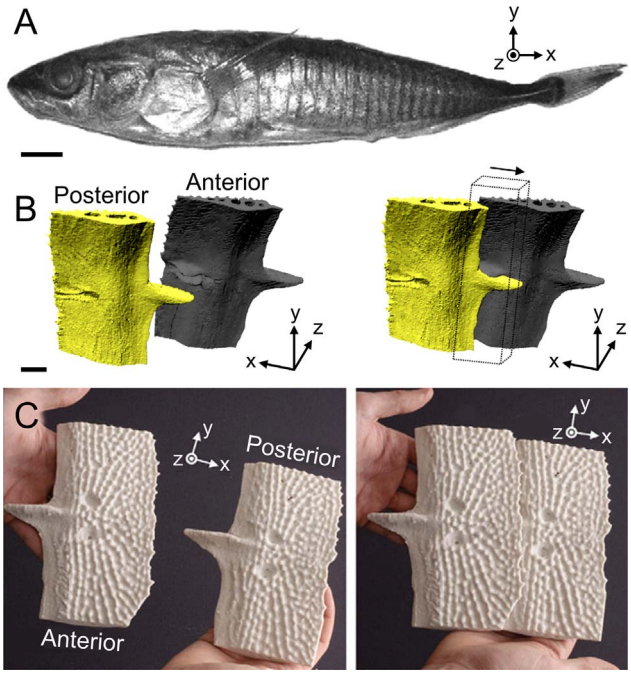

Fig. 3. Bony plates of a threespine stickleback. **(A)** Image of a threespine stickleback fish (*Gasterosteus aculeatus*); **(B)** micro-computed tomography images and **(C)** 3D-printed models of two segmented bony plates, illustrating the peg-and-socket articulation between the anterior and posterior plates. The arrow in (B) indicates the direction of insertion of the peg-and-socket joint. The coordinate axes indicate the anteroposterior (x), ventrodorsal (y), and lateral (z) directions, with respect to the body of the fish. Scale bars: (A & B) 500 μm. Images adapted from (Song et al., 2010).

tetraodontiformes, such as boxfishes (Besseau and Bouligand, 1998; Yang et al., 2015). The scutes of a boxfish carapace (not to be confused with the 'scutes' of catfishes (Ebenstein et al., 2015; Sire, 1993) which are in fact 'bony plates') exist in the form of tessellating, flattened polygonal (mostly hexagonal) surface-mineralized disks covering an underlying network of non-mineralized collagen (Fig. 2**D**) (Yang et al., 2015). The interfaces between the mineralized regions of the scutes are strongly abutted, forming interdigitated, but disjoined sutures that do not contain any connective tissues (Yang et al., 2015) (e.g., Sharpey's fibers often join the mineralized scutes of geometrically similar armors, such as armadillo osteoderms (Chen et al., 2011; Vickaryous and Hall, 2006)). These unusual sutured interfaces are thought to accommodate pressure changes associated with the animal's habitat or growth (Yang et al., 2015), similar to the cranial sutures common in many mammals (Hubbard et al., 1971; Jaslow, 1990).

3.5. Bony plates

Bony plates, as described here, are composed entirely of bone (and distinguished from 'carapace scutes') and often protect gasterosteiformes and syngnathiformes, such as sticklebacks and seahorses (Ehrlich, 2015; Sire and Huysseune, 2003). The primary difference between these heavily-mineralized plates and other bony-like fish armors (e.g., scutes) are their uniformly mineralized bone-like composition and their augmented peg-and-socket joints (Fig. 2**E**) (Neutens et al., 2014; Porter et al., 2013; Song et al., 2010). In seahorses, for instance, both overlapping and peg-and-socket joints allow for the serial articulation of multiple adjacent plates, forming a highly-interlocked, yet flexible protective armor (Hale, 1996; Neutens et al., 2014; Porter et al., 2013; Praet et al., 2012). Although bony plates are derived from the dermis (Sire et al., 2009), they sometimes also function as an integral part of the musculoskeletal system, providing added body mobility through direct muscular interactions (Neutens et al., 2014; Praet et al., 2012).

4. Multifunctional mechanics of selected bioinspired systems

Over the past several decades, several studies have revealed the combined protective strength, flexibility, and other biomechanical functions of a variety of natural dermal armors (Vickaryous and Sire, 2009; Yang et al., 2013a), including various types of fish scales (Ehrlich, 2015; Sire et al., 2009; Vernerey and Barthelat, 2010; Zhu et al., 2012), carapace scutes (Besseau and Bouligand, 1998; Yang et al., 2015), and bony plates (Hale, 1996; Neutens et al., 2014; Porter et al., 2013). However, one of the first reports to employ 3D-printing to study an armored fish was carried out by Song et al. (2010) on the threespine stickleback (*Gasterosteus aculeatus*) shown in Fig. 3**A**. Sticklebacks are a fascinating clade of fishes covered by thick bony plates (Song et al., 2010), which also happen to serve as model systems for studies of ecology and evolution due to their rapid loss of armor as they migrate from marine to freshwaters (Barrett et al., 2008; Jones et al., 2012). The bony plates are serially connected through peg-and-socket joints to facilitate body mobility. Using micro-computed tomography (micro-CT) data (Fig. 3**B**), 3D-printed scaled-up replicas of the plates (Fig. 3**C**) were used not only to better visualize the interlocking armor, its morphology and protective function, but also to more accurately evaluate the degrees of freedom allowed by the peg-and-socket joints (Song et al., 2010). The unique ellipsoidal-like joints allow

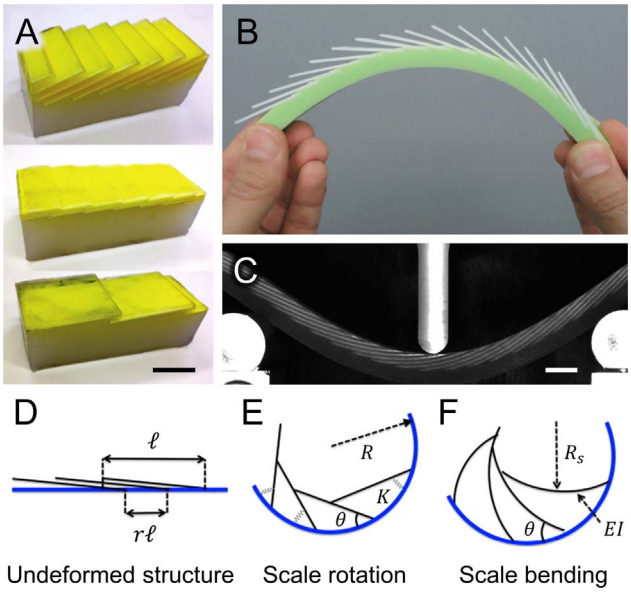

Fig. 4. Elasmoid scales provide body mobility and puncture resistance. **(A)** Three representative 3D-printed models used to evaluate the effects of scale size, inclination, and overlap; **(B)** 3D-printed model of overlapping scales used to validate analytical models describing the effect of frictional sliding during bending; **(C)** multi-material 3D-printed model of hard scales embedded in a soft substrate subjected to 3-point bending. **(D–F)** Diagrams illustrating the two-dimensional micromechanical behavior of overlapping fishscales in concave bending, which are dependent on the rotation and bending stiffness of the scales. Symbols in (D–F): scale length (ℓ), separation distance ($r\ell$), radius of curvature of the skin (R) and scale (R_s), scale rotation angle (θ), scale attachment stiffness (K), and scale rigidity (EI). Scale bars: (A) 25 mm; (C) 10 mm. Images adapted from (A) (Browning et al., 2013); (B) (Ghosh et al., 2014); (C) (Rudykh et al., 2015); (D–F) (Vernerey and Barthelat, 2014).

for multiple degrees of freedom: one translational, along the major axis of the peg (illustrated by the arrow in Fig. 3**B**), and three rotational, one along the major axis and two more constrained rotations along the minor axes of the peg. Thus, it was demonstrated that the biomechanics of natural systems can be explained non-destructively through virtual models (via micro-CT) and physical prototypes (via 3D-printing).

4.1. Flexible protection

A few research groups (Browning et al., 2013; Ghosh et al., 2014, 2015; Rudykh and Boyce, 2014b; Rudykh et al., 2015) have recently built 3D-printed models inspired by the overlapping scales of modern teleost fishes (Fig. 4**A-C**). These models have been used as analogues to better understand the mechanics that govern the functions of puncture resistance and body flexibility in the living animals as well as to inform potential engineering applications. By modifying key parameters, such as plate stiffness, length and thickness, imbrication distance and angle of inclination, these authors (Browning et al., 2013; Ghosh et al., 2014, 2015; Rudykh and Boyce, 2014b; Rudykh et al., 2015) have revealed many of the underlying mechanisms that dictate the multiple, often opposing properties of combined protection and flexibility.

In each of these studies (Browning et al., 2013; Ghosh et al., 2014, 2015; Rudykh and Boyce, 2014b; Rudykh et al., 2015) 3D-printing was employed to fabricate rigid 'scales' anchored into a soft supporting 'dermal' layer, mimicking the basic architecture of elasmoid-like armors (Fig. 4**A–C**). Browning et al. (2013) fabricated scales by 3D-printing, and then cast them into a silicon rubber which served as a flexible base. The physical models were used to compare several biologically-relevant configurations of scale volume fraction (ϕ), a metric dependent on the scale aspect ratio (R_a), spatial overlap (K_d) and angle of inclination (θ): $\phi = \frac{\tan^2\theta+1}{K_d R_a \tan\theta}$; Fig. 4**A** shows three of the configurations investigated. Ghosh et al. (2014) glued 3D-printed scales onto a flexible silicon base (Fig. 4**B**), which was used to experimentally verify analytical models describing the nonlinear mechanical behavior of inter-scale contact due to frictional sliding between adjacent scales in bending. Rudykh et al. (2015) used a multi-material 3D-printer to form composites with microstructures consisting of rigid scale-like layers embedded in a soft flexible matrix (Fig. 4**C**), where the angle of inclination and volume fraction of the stiff phase (i.e., scales) were compared.

Each of the biomimetic prototypes were subjected to different modes of loading (Fig. 4**A–C**), including plane strain compression (Browning et al., 2013), 3-point bending (Ghosh et al., 2014; Rudykh et al., 2015), and indentation (Rudykh et al., 2015). The resulting mechanical behaviors of the models (also investigated via finite element analyses) reveal that scale rotation, bending, and frictional sliding, as well as tissue shear deformations within the compliant phase, control the overall mechanical behavior of the overlapping armors, agreeing with generalized micromechanical models developed to predict the behavior of fishscale structures (Vernerey and Barthelat, 2010, 2014). Basic assumptions for the models are shown in Fig. 4**D–F** (Vernerey and Barthelat, 2014), where the overall curvature of a scaled skin (with scales of length ℓ and separation distance $r\ell$ (Fig. 4**D**)) subjected to concave bending results from the normalized curvatures caused by scale rotation ($\bar{\kappa}_r$, which depends on the stiffness of scale attachment, K (Fig. 4**E**)) and from scale bending ($\bar{\kappa}_b$, which depends on the stiffness of the individual scales, EI (Fig. 4**F**)). As a result, distinct mechanical behaviors (e.g., scale rotation or bending) may dominate depending on the different morphologies and material properties of the hard and soft phases. For instance, scale rotation dominates for scales with small aspect ratios, while bending dominates for larger aspect ratios (Browning et al., 2013), suggesting that varying combinations of properties generate varying behaviors, and hence tradeoffs in flexibility and protection. To further explain this phenomenon, Rudykh et al. (2015) developed a new metric to quantify these mutually-exclusive properties known as the 'protecto-flexibility' of a material: $\Psi = C^{(p)}/C^{(b)}$, which is the ratio of penetration stiffness ($C^{(p)}=P/\Delta$) to bending stiffness ($C^{(b)}=M/\varphi$), where P and Δ are the normalized indentation force and depth, and M and φ are the normalized bending moment and angle, respectively. Thus, a wide range of composite properties are possible by fine tuning the geometric and material properties of overlapping scaled-structures, explaining why different scale configurations are found within different species and anatomical locations of fishes – to provide specific combinations of protection and flexibility.

In addition to the relative high flexibility afforded by the overlapping nature of elasmoid scales, which allows for unimpeded body flexure during swimming, rotation and bending of the scales can store and release energy to aid in locomotion (Vernerey and Barthelat, 2014). Similar mechanisms in the skins and scales of various fishes have been described as 'external tendons' that restitute energy and regulate body undulations (Hebrank, 1980; Hebrank and Hebrank, 1986; Long et al., 1996; Vernerey and Barthelat, 2010, 2014; Wainwright et al., 1978). Interestingly, this mechanism was exploited in synthetic microstructures, where large rotational motions were obtained as an effect of small point loads, showing promise as a novel actuator design for soft robotics applications (Rudykh and Boyce, 2014b).

In another recent study, Duro-Royo et al. (2015) 3D-printed replicas of ganoid fish scales to investigate their potential for human body armor (Fig. 5). The transition of functionality (from protection to flexibility) was examined to determine how the local, regional, and global design of the armor along the body of a bichir (*Polypterus senegalus*) could be adapted to cover different body curvatures, for instance, of a human shoulder (Duro-Royo et al., 2015). In an attempt to understand the tradeoffs necessary to provide tailored protection and flexibility, it was found that the size of the joints of the ganoid scales in *P. senegalus* become reduced from head to tail to permit

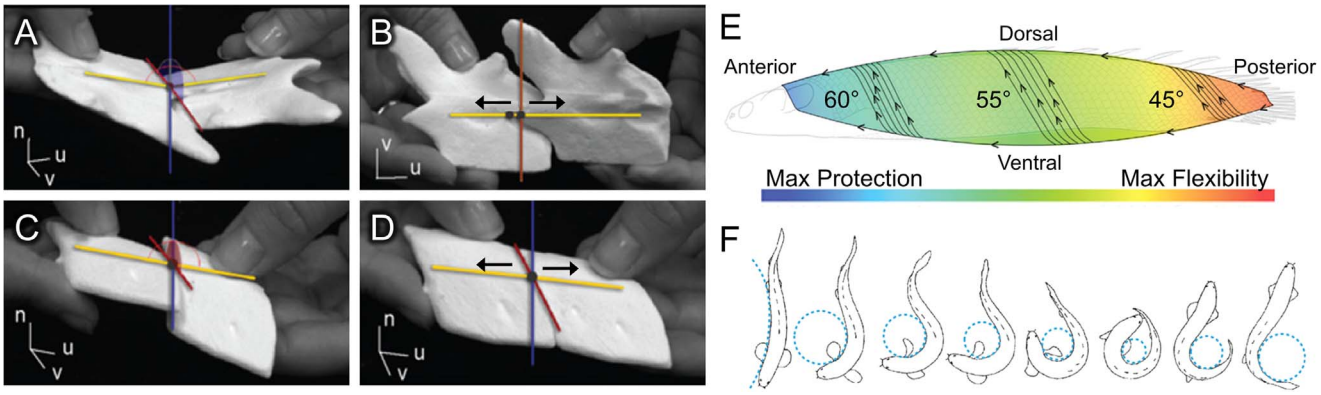

Fig. 5. Ganoid scales provide protection and flexibility. **(A-D)** 3D-printed replicas of scales from near the head (A, B) and tail (C, D) of a bichir fish (*Polypterus senegalus*); **(E)** schematic illustrating the transition from protection near the head of the fish in blue to flexibility near the tail of the fish in red. **(F)** Illustrations of different body curvatures observed in swimming fishes. The arrows in (B & D) indicate the direction of insertion of the peg-and-socket joints. The coordinate axes indicate the anteroposterior (u), ventrodorsal (v), and lateral (n) directions, with respect to the body of the fish. Images adapted from (Duro-Royo et al., 2015). (For interpretation of the references to color in this figure legend, the reader is referred to the web version of this article.)

greater mobility along the paraserial axis (parallel to the peg-and-socket joints) and interserial axis (parallel to the overlapping joints) (Duro-Royo et al., 2015; Varshney et al., 2015). The larger, more prominent peg-and-socket joints and anterior processes near the head of the fish provide greater protection (Fig. 5**A, B** and blue region in Fig. 5**E**), while those near the tail are smaller and less prominent to permit more flexibility (Fig. 5**C,D** and red region in Fig. 5**E**) (Duro-Royo et al., 2015; Varshney et al., 2015). Furthermore, multiple neighboring scales are arranged into rings that warp around the trunk of the fish. These structural rings are slanted in such a way, as shown in Fig. 5**E**, in order to mitigate body torsion, yet allow for adequate bending in steady-state swimming (with large radii of curvature) and other fast-start maneuvers (with small radii of curvature), as seen in Fig. 5**F** (Duro-Royo et al., 2015).

The effect of the interactions between neighboring scales can be further highlighted by comparing the performance of scales with very simple geometries to those of increasing complexity that contain interlocking features. Fig. 6**A** shows a 5×5 array of simple square scales made of a stiff ABS plastic fabricated by a 3D printer. The scales, resting on a softer substrate, were indented by a sharp needle. Because of the relatively high strength of the scales and the high compliance of the substrate, the scaled system fails by tilting of the indented scale. This dangerous failure mode was recently identified in gar fish (covered with ganoid scales) and studied in detail using glass plates on silicone and contact mechanics (Martini and Barthelat, 2016). An important implication of these observations is that even scales made of the strongest materials can be relatively easily defeated by tilting, if no preventative mechanisms are introduced. Fig. 6**B** shows the same system, but in this case the sides of the scales were slanted at ± 45° angles, so as to generate a topologically interlocked array of scales (Dyskin et al., 2003; Khandelwal et al., 2012; Mirkhalaf et al., 2016). This enrichment to the geometry of the scales generates interlocking of the scales under puncture, which delays the tilting of the indented scale and increases the puncture resistance by a factor of four. Fig. 6**C** highlights the improvement in puncture resistance for the topologically interlocked array of scales. The improvement was explained by the engagement of the neighboring scales due to the slanted interfaces, as captured by in-situ imaging of the array of scales during puncture tests.

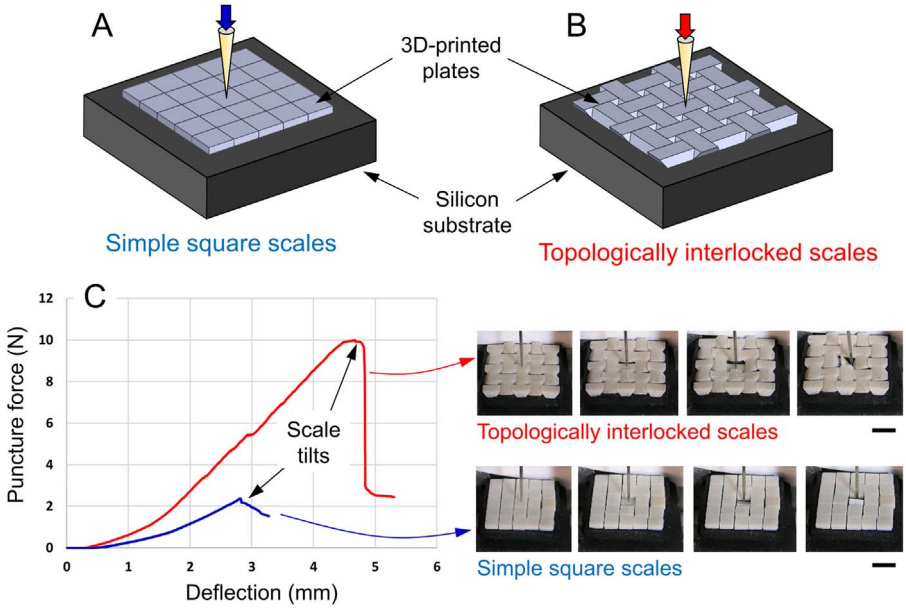

Fig. 6. Effect of scale geometry on puncture resistance. **(A)** A 5×5 array of simple square scales made of stiff ABS plastic resting on a softer silicon substrate, punctured by a sharp steel needle; **(B)** the same system, with the addition of 45° angles on the sides of the scales to generate topological interlocking between the scales. **(C)** Puncture force-deflection curves for simple and interlocked scales with associated sequences of pictures. Both systems fail by sudden tilting of the indented scale. However, tilting is delayed in the interlocked scales, which increases the puncture resistance by a factor of four. Scale bars: 10 mm. Images courtesy of F.B.

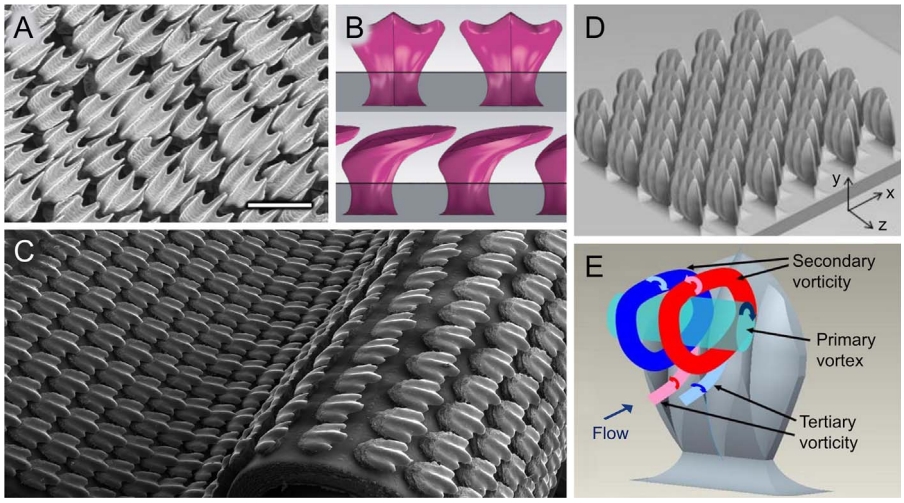

Fig. 7. Placoid scales (dermal denticles) reduce drag in shark skins. **(A)** Scanning electron micrograph of a natural shark skin (*Sphyrna tiburo*); **(B)** computer model of biomimetic denticles designed for 3D-printing; **(C)** micrograph of a biomimetic shark skin, showing scale engagement in concave bending and scale separation in convex bending. **(D)** Image of a computer-rendered model of bristled scales used to create a synthetic prototype for experimental testing; **(E)** schematic illustration of the fluid roller bearing effect of drag reduction by bristled scales, showing the primary, secondary, and tertiary vorticities. The axes in (D) indicate the anteroposterior (x), lateral (y), and ventrodorsal (z) directions. Scale bars: (A) 200 μm; (C & D) each denticle is scaled up from the natural ~200 μm to (C) ~1.5 mm long and (D) ~20 mm long. Images adapted from (A–C) (Wen et al., 2014) and (D & E) (Lang et al., 2008).

The design space for interlocking scales is vast and the geometrical features that may enhance the puncture resistance of the scales have not been fully identified yet. 3D printing, together with numerical modeling and bioinspiration, will likely play an increasingly important role in the exploration and search of optimum designs.

4.2. Hydrodynamics

Most fishes secrete a thin layer of mucus over their skin, which acts like a lubricant to resist abrasion, reduce frictional fluid drag during swimming, and protect their skin from microbial proliferation (Shephard, 1994; Sudo et al., 2002; Waghmare et al., 2014). Many sharks, however, rely on a more structural means for protection, drag reduction and anti-biofouling. Their skin is covered with placoid scales having unique external profiles that resemble tiny hydrofoils (Fig. 7**A**) (Wen et al., 2014). The scales of many other fishes also have microscopic surface ridges (on the order of 10–100 μm) that reduce drag (Fletcher et al., 2014; Sudo et al., 2002), but generally the effect is less pronounced. In addition to drag reduction (discussed below), the ribbed surfaces of most fish and shark scales help resist biofouling because the spacing of the ribs are such that micro-organisms cannot easily attach and grow (Emily and Geoffrey, 2009). There are many bioinspired self-cleaning surfaces that utilize similar mechanisms (Kirschner and Brennan, 2012; Liu and Jiang, 2012; Nishimoto and Bhushan, 2013); however, to the best of our knowledge there are no reports of such 3D-printed structures. This is likely due to current limitations on the resolution of most 3D-printing processes. Also, other processes have proven effective in making anti-biofouling surfaces (Kirschner and Brennan, 2012; Liu and Jiang, 2012; Nishimoto and Bhushan, 2013), such as the commercial product, Sharklet (Sharklet Technologies, 2007), a synthetic surface that mimics the micro-architecture of shark skin.

In two recent studies (Wen et al., 2014, 2015), comparative biomimetic shark skins were fabricated via multi-material 3D-printing and tested in flow tank experiments to reveal the hydrodynamic properties of dermal denticles. The synthetic skins were composed of a soft plate-like base covered by hard denticle-like ornaments with varying spacing and patterning (Fig. 7**C**). The artificial denticles were modeled as idealized hydrofoils with characteristic undercuts, overlaps and overhangs, as observed in the natural scales (Fig. 7**B**). Using a mechanical flapping device, the synthetic skins were oscillated dynamically at different heave frequencies, amplitudes, and pitch angles to compare the hydrodynamic loading, swimming speeds, power consumption and cost of transport of the different skins. When compared with a smooth control surface, an artificial skin covered with tiny hydrofoils generated a stronger leading edge vortex, which is suggested to improve thrust (Wen et al., 2014). The biomimetic skin also reduced static drag up to 8.7% (as compared with the smooth control), depending on the specific heave and flow conditions (Wen et al., 2014). Moreover, the interaction of adjacent denticles near the distal end of some sharks aids in undulatory locomotion when their skin flexes (Motta et al., 2012; Oeffner and Lauder, 2012; Wainwright et al., 1978), presenting an energy restitution mechanism similar to that of overlapping elasmoid scales (discussed above). This effect of skin curvature on the contact and interaction of scales in concave bending, as opposed to convex bending, is illustrated in Fig. 7**C** (Wen et al., 2014). It was further explained, by Wen et al. (2015), by changing the denticle spacing (spaced or overlapped) and patterning (linear or staggered) of several synthetic skins. They revealed that a staggered-overlapping pattern of denticles resulted in higher self-propelled swimming speeds, more than 20% faster on average than those with linearly-overlapped, periodically-spaced, and no denticles (smooth control).

In earlier studies (Bechert et al., 2000; Lang et al., 2008), the effects of the scales' anchorage (which is flexible) and angle of attack (which is passively controlled) were investigated using natural and artificial skins; the artificial skins were fabricated by different micro-fabrication techniques (e.g., rapid prototyping (Lang et al., 2008) and solution casting (Bechert et al., 2000)). Although not 3D-printed, Bechert et al. (2000) created two models of shark skin-inspired surfaces: stationary riblets and movable scales. Flow experiments on these structures confirmed that the exterior shape of the riblets and the flexible anchorage of the scales could enhanced their drag reduction performance (Bechert et al., 2000). In a more recent study, Lang et al. (2008) used rapid prototyping to create a synthetic model of bristled (erect) scales (Fig. 7**D**). They found that the bristled scales form embedded vortices between them to reduce drag through the 'fluid roller bearing' effect (Fig. 7**E**), which decreases contact between the fluid flow and the solid surface.

In another study on fish hydrodynamics, Van Wassenbergh et al. (2015) 3D-printed replicas of the carapaces (outer profiles) of two ostraciid fishes (a trunkfish, *Rhinesomus triqueter*, and a boxfish,

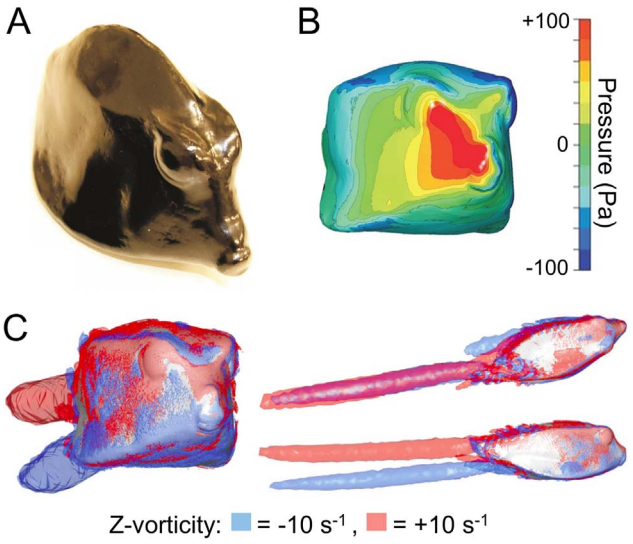

Fig. 8. The shape of a boxfish carapace enhances swimming manueverability. **(A)** 3D-printed model of a boxfish carapace (~60 mm wide). **(B & C)** Computational fluid dynamics models of (B) the lead-edge pressure waves and (C) the trailing-edge vortices induced during swimming of a boxfish (*Ostracion cubicus*). The color scheme in (B) illustrates the distribution of negative pressure (blue) to postitive pressure (red) on the leading-edge of the carapace. The color scheme in (B) illustrates vorticity flows in the anti-clockwise (blue) and clockwise (red) directions for the front (left), dorsal (top, right) and lateral (bottom, right) views. Images adapted from (Van Wassenbergh et al., 2015). (For interpretation of the references to color in this figure legend, the reader is referred to the web version of this article.)

Ostracion cubicus) to resolve how their unique body shapes contribute to their high maneuverability. Fig. 8 shows images of a 3D-printed boxfish model (Fig. 8**A**) and computational fluid dynamics (CFD) simulations of the pressure distributions (Fig. 8**B**) and the vorticities induced by the fish's boxy shape (Fig. 8**C**) (Van Wassenbergh et al., 2015). Contrary to previous work (Bartol et al., 2005; Bartol et al., 2003; Bartol et al., 2002), it was found that the boxy shape of the carapace generates strong destabilizing moments produced by pressure waves at its leading-edge (Fig. 8**B**) that counteract the stabilizing moments generated by trailing-edge vorticities produced by its keels (Fig. 8**C**). These destabilizing forces increase the overall drag experienced by the fish (Van Wassenbergh et al., 2015); however, they also amplify the fish's maneuverability, allowing it to turn on a dime, literally 180° over a single body length (Walker, 2000) – an impressive and vitally important feat given boxfishes' obstacle-strewn habitat of coral reefs. The 3D-printed models in this study (Van Wassenbergh et al., 2015) were used to directly measure the forces acting on the carapace under a variety of ecologically-relevant flow conditions, and thus verify the computational models that resolved the boxfish paradox: how sacrifices in stability (via trailing-edge vorticities) permit greater maneuverability (via leading-edge pressure waves).

4.3. Body support

Not only do boxfishes exhibit impressive maneuverability due to the unique shape of their carapace (Van Wassenbergh et al., 2015), they also lack a fully developed internal skeleton (e.g., ribs) (Nelson, 2006). Instead, their bodies are supported by the external carapace (and a central vertebral column) (Besseau and Bouligand, 1998; Yang et al., 2015). Micro-CT images of the carapace's hierarchical structure are shown in Fig. 9**A–C**, where it consists of several tessellating scutes, most often in the form of flattened hexagons, that are connected by zigzag-like triangular sutures (Yang et al., 2015). To test the proposed hypothesis that sutured interfaces help accommodate external loadings (e.g., due to their environment, growth, or predatory attacks) (Yang et al., 2015), three hypothetical models representative of a boxfish

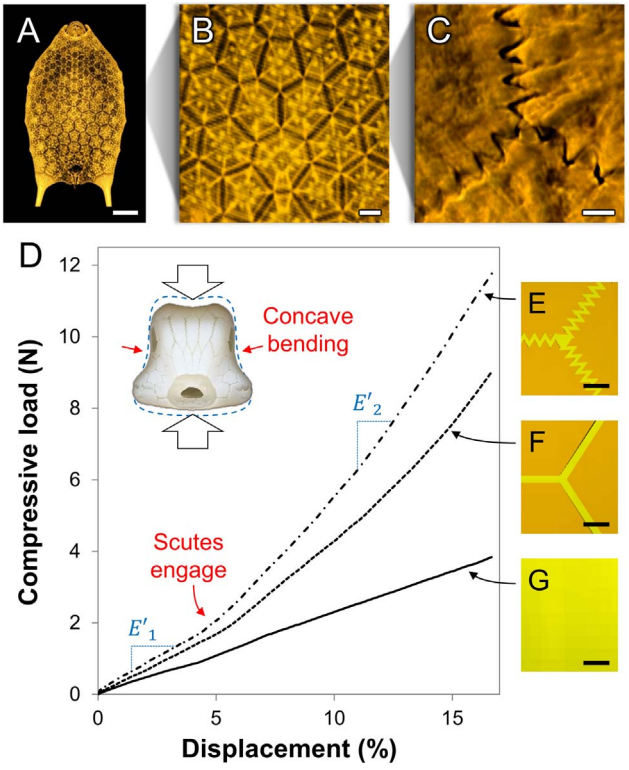

Fig. 9. Carapace scutes provide body support in boxfishes. **(A–C)** Micro-computed tomography images of the hierarchical organization of a boxfish carapace (*Lactoria cornuta*), showing its (A) ventral surface, (B) tessellation pattern of predominantly hexagonal scutes, and (C) zigzag-like sutures between adjacenet scutes. **(D)** Load-displacement curves illustrating the compressive behaviors of three hypothetical models of 3D-printed boxfish carapaces. The inset (top, left) shows a representative 3D-printed model of a boxfish carapace (~70 mm wide) that was compressed ~15%, where the blue outline shows its orginal shape before loading. The slopes of the load-displacement curves before and after the scutes engage, which is a result of concave bending of the carapace sides, are denoted by the apparent moduli, E'_1 and E'_2. **(E–G)** Magnified models of the three hypothetical carapaces tested, two with a biomimietc armor (orange) covering a flexible skin (yellow) having (E) sutured interfaces or (F) flat interfaces, and another with (G) a flexible skin only. Scale bars: (A) 5 mm; (B) 1 mm; (C) 50 μm; (E–G) 2 mm. Images adapted from (A–C) (Yang et al., 2015) and (D–G) courtesy of M.M.P. (For interpretation of the references to color in this figure legend, the reader is referred to the web version of this article.)

carapace were created with a multi-material 3D-printer (Fig. 9**E–G**): (i) a soft, flexible body (yellow) covered with tessellating scutes having triangular sutures (orange) (Fig. 9**E**); (ii) a soft, flexible body (yellow) covered with scutes having flat interfaces (orange) (Fig. 9**F**); (iii) a soft flexible body only (yellow) (Fig. 9**G**). In all three models, the thicknesses of the layer of soft skin (i.e., the flexible base having a tensile strength of ~1 MPa, shown in yellow) and the layer of rigid hexagonal scutes (i.e., those with and without sutures having a tensile strength of ~60 MPa, shown in orange) were kept constant such that the rigid exterior made up 20% of the total carapace thickness, similar to that observed in nature (Yang et al., 2015). For illustrative purposes, Fig. 9**D** shows load-displacement curves of the three 3D-printed carapaces subjected to unilateral compressive loading (Kenneson, 2016). The inset shows a 3D-printed model of the carapace under a compressive displacement of ~15%.

As seen in Fig. 9, the trapezoidal-shaped body of the 3D-printed boxfish model caused the lateral walls of its carapace (which are initially concave, as in most boxfish species (Marcroft, 2015)) to bend under the compressive load. This causes the outer scutes of the carapace to engage under compression, at which point the apparent stiffnesses of the models (E'_1 and E'_2, the slopes of the load-displacement curves) begin to deviate, where $E'_2 > E'_1$. As expected, the presence and engagement of the rigid scutes covering the exterior of

the carapace enhances its strength and stiffness considerably, by more than two times that of the carapace with no armor. Adding the triangular sutures to the scutes further enhances its compressive resistance, increasing more than two and one half times in strength and four times in stiffness (after the sutures engage), compared to the model with no armor. This result is likely due to the fact that the sutures not only increase surface area contact between the scutes, but also act as a sort of locking mechanism that prevents slip due to shearing between adjacent scutes (Yang et al., 2015). While these results indicate that the sutures found in boxfish carapaces could accommodate pressure changes or mitigate compressive failure due to their underwater habitat and growth or predatory attacks (Kenneson, 2016), further research is necessary to fully validate these hypotheses (the topic of ongoing work). Regardless, we demonstrate here that running preliminary mechanical tests on 3D-printed models can reveal much information about their behaviors, which can help inform subsequent paths of scientific inquiry (e.g., testing different suture geometries).

In related work, Li et al. developed detailed micromechanical models to predict the strength and stiffness of sutured interfaces with varying geometries of first-order (Li et al., 2011), hierarchical (Li et al., 2012), and arbitrary (Li et al., 2013) organization, including a triangular suture geometry reminiscent of that observed in the boxfish. Fig. 10 shows images of 3D-printed models used to explore the mechanical behaviors of idealized first-order (Fig. 10**A**) (Lin et al., 2014a) and hierarchical (Fig. 10**B**) (Lin et al., 2014b) geometries with anti-trapezoidal, rectangular, trapezoidal, and triangular interfaces.

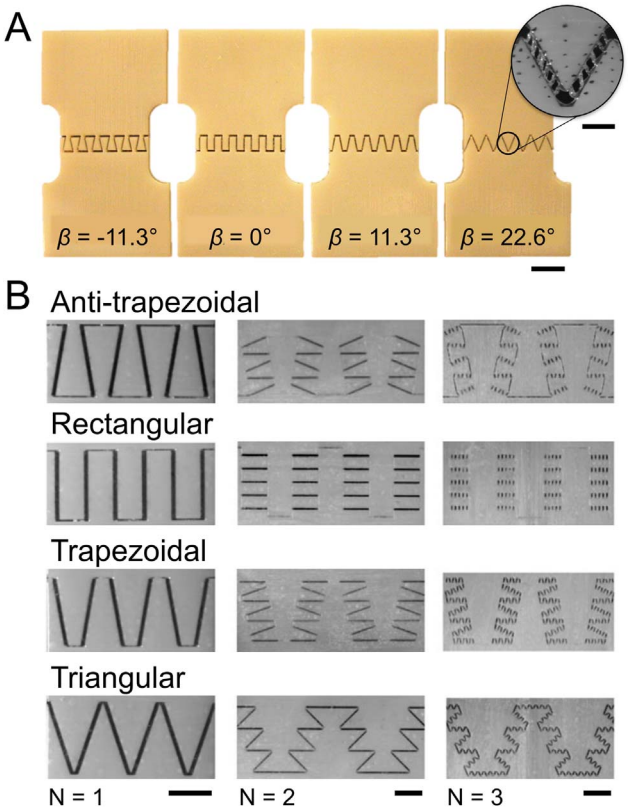

Fig. 10. Suture geometries and hierarchies provide mechanical strength, stiffness, and toughness. **(A)** 3D-printed samples with first-order sutures, where β describes the suture angle measured with respect to the vertical axis of anti-trapezoidal (−11.3°), rectangular (0°), trapezoidal (11.3°), and triangular (22.6°) geometries. The inset (top, right) shows stretching of the softer interfacial layer that bonds the traingular sutures when subject to tension. **(B)** 3D-printed samples with varying levels of suture hierarchy, where N describes the level of hierarchy, as first (1), second (2), or third (3) order. Scale bars: (A) 10 mm (inset: 5 mm); (B) 10 mm. Images adapted from (A) (Lin et al., 2014a) and (B) (Lin et al., 2014b).

Interestingly, the triangular geometry exhibits the highest tensile and shear strength, stiffness, and fracture toughness when compared to the other geometries because the stresses are uniformly distributed through its teeth and interfacial layers (Li et al., 2013; Lin et al., 2014a); and, including additional levels of fractal-like hierarchy nonlinearly amplifies their mechanical behaviors (Li et al., 2012; Lin et al., 2014b). In tension, the slanted geometry of the triangular sutures more evenly distributes the normal tensile and tangential shear stresses across its zigzag-like interface. In contrast, rectangular sutures (and to a lesser degree, trapezoidal sutures) have more horizontally and vertically-oriented interfaces that carry the normal tensile and tangential shear stresses, respectively. Thus, triangular sutures are often found in biological structures that require a more uniform distribution of stresses through their interfaces.

One difference between the sutures found in the boxfish carapace and these models, however, is the inclusion of a soft interfacial layer in the models (see inset, Fig. 10**A**) that connects the hard skeletal 'teeth' of the joints (Lin et al., 2014a, 2014b). Such a compliant interface is characteristic of many sutures observed in nature, which both adheres the skeletal plates together and provides some flexibility (Hubbard et al., 1971; Jaslow, 1990). Further, while the scutes of the boxfish carapace are abutted together along a zigzag-like interface (Fig. 9**C**), the suture wavelength (~65 μm) and angle (~50°) are significantly different from the predicted optimal values derived for similar bone-like materials (Li et al., 2011) and other sutures found in nature (Li et al., 2013), which typically exhibit values on the order of 100–1000 μm and 5–25°, respectively. This large disparity in suture design is likely due to the different modes of loading commonly encountered by the different organisms (Yang et al., 2015). As illustrated in Fig. 9**D**, the boxfish carapace is likely to buckle and bend (due to its natural concavity) in response to the lateral compression of a predatory attack, which could cause the outer layer of its mineralized scutes to compress in contact – a likely explanation for the different suture designs. Once again, the interlocking mechanism of contacting sutures not only prevents shear between adjacent scutes, but also stiffens the joints.

Similar to boxfishes, seahorses (Fig. 11**A**) and related syngnathid fishes have bony plated armors that provide skeletal body support (Hale, 1996; Neutens et al., 2014; Porter et al., 2013). The unique square structure of a seahorse tail (Fig. 11**B**) protects against impact and crushing via overlapping joints between adjacent plates that slide linearly when compressed (Fig. 11**C**) (Porter et al., 2015). This combination of overlapping joints with peg-and-socket articulations between the square tail segments also restricts significant body torsion, yet allows these fishes to bend their tails for the added function of prehensility.

4.4. Tail prehensility

Seahorses and related pipehorses are unusual fishes that possess prehensile tails (Neutens et al., 2014), capable of grasping and holding on to aquatic vegetation. Their tails do not possess caudal fins, and they are made up of bony plates that form unique articulating structures, often arranged into ring-like segments (Fig. 11**A–C**) (Hale, 1996). Muscles in their tails are attached to the bony plates and transfer forces from the vertebral column to facilitate motion (Praet et al., 2012). Even though seahorse tails can bend in different directions (ventral, dorsal, and lateral), they coil up (forming a logarithmic spiral) in the ventral direction to a greater degree (Neutens et al., 2014). This difference in bending capacity is due to the geometric design of the tail plates (Porter et al., 2013; Praet et al., 2012); the ventral plates always overlap the dorsal plates and a plate skew (angular shift between the ventral and dorsal plates) increases as the tail tapers in size towards the distal tip. To reveal why the plates of a seahorse tail are arranged in the form of a square prism rather than a cylinder, Porter et al. (2015) designed, built, and tested two 3D-printed prototypes: one that mimicked the natural seahorse tail structure (an idealized square-prism) and another of a

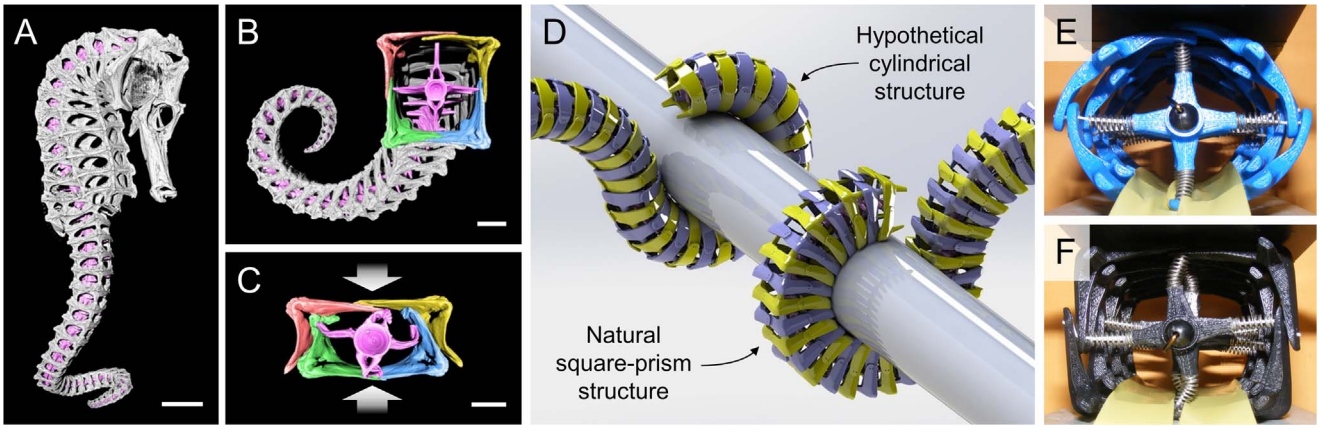

Fig. 11. Bony plates facilitate tail prehensility in seahorses. **(A-C)** Micro-computed tomographs of (A) a seahorse (*Hippocampus reidi*) and its tail in (B) bending, twisting, and (C) compression. For clarity, the vertebral column is colored magenta, and the bony plates are colored red, yellow, blue, and green. **(D)** Computer-generated images of a hypothetical cylindrical model and a natural square-prism model of a seahorse tail wrapped around a cylinder, illustrating their respective surface contact when grasping. **(E, F)** Images of 3D-printed prototypes compressed just before failure, which occurs when the spring struts disjoin from the 3D-printed plates, illustrating the (E) rotational hinge and (F) linear sliding mechanisms that occur at the overlapping joints of the cylindrical and square-prism structures, respectively. Scale bars: (A) 10 mm; (B & C) 2 mm; (E & F) 3D-printed models are ~60 mm wide. Images adapted from (A–C, E, F) (Porter et al., 2015) and (D) courtesy of M.M.P. (For interpretation of the references to color in this figure legend, the reader is referred to the web version of this article.)

hypothetical cylindrical structure (Fig. 11**D–F**). Both prototypes served as simplified models of an armored tail skeleton, consisting of six segmented-rings of equal plate size, no plate skew, and an alternating overlap sequence, allowing the prototypes to bend equally in all directions. Through a series of mechanical tests, the two structures were compared according to their performance in bending, twisting, impact and crushing.

Articulation in the 3D-printed prototypes was primarily governed by three distinct joints: ball-and-socket, peg-and-socket, and gliding. The ball-and-socket joints of the vertebrae constrain bending (Porter et al., 2015). However, it was found that the cylindrical prototype was slightly less constrained in bending, when compared with the square prototype, because the peg-and-socket joints located at the ring corners of the latter restricted motion between adjacent segments to a greater degree. In twisting, the cylindrical structure exhibited inter-segmental rotations approximately twice that of the square structure (Porter et al., 2015). The peg-and-socket joints also facilitate an additional articulatory reorganization mechanism that allowed the square prototype to return to a neutral 'resting' position upon excessive manipulation. In contrast, the circular prototype did not return to a straightened position upon extensive deformation. This restoring mechanism could help protect the fishes from soft tissue damage caused by over-twisting and allow them to 'rest' without expending energy (Porter et al., 2015). Furthermore, the square structure has a flat exterior surface, which provides a greater contact area for grasping, as shown in Fig. 11**D**. It is suggested that seahorses likely evolved the ability to grasp, in part owing to the unique combination of mechanical mechanisms afforded by the square-prism structure (as opposed to a hypothetical cylindrical structure).

The ability of the square prototype to restore its shape was further observed when the prototypes were crushed or impacted with a rubber mallet (Porter et al., 2015). The linear sliding that occurs in the square structure subjected to compression is permitted by the flat shape of its overlapping joints (Fig. 11**F**). Conversely, the cylindrical prototype expands in the transverse direction when compressed, forming a rotational hinge at the overlapping joints, which transforms its cross-sectional shape from circular to elliptical (Fig. 11**E**). To better understand the protective function of the gliding joints, solid rings with square and circular cross-sections were also 3D-printed and crushed (Porter et al., 2015). Upon exceeding the yield stress of the ring material, plastic deformation was observed at the locations of maximum stress causing the onset of plastic hinges. Remarkably, the gliding joints in a seahorse tail are located at the same position as these plastic hinge zones, which occur at the side midsections of a square ring. By adding joints at the locations of predicted failure (for solid rings), the square prototype absorbed much more energy when crushed, and outperformed its cylindrical counterpart as a protective armor, exhibiting a compressive response approximately three times stiffer, four times stronger, and one and one half times more compliant.

5. Concluding remarks

Over the past few years, several research groups 3D-printed biomimetic models of various fish armors to investigate their different functionalities. Mimicking the overlapping arrangement of elasmoid-like (Browning et al., 2013; Ghosh et al., 2014; Rudykh et al., 2015) and ganoid-like (Duro-Royo et al., 2015) scales revealed that scale rotation, bending, and frictional sliding facilitates varying amounts of resistance to penetration (protection) and body mobility (flexibility), while simple geometries that create a topological interlocking effect between adjacent scales further increases their penetration resistance. Comparative testing of biomimetic shark skins showed that adding denticle-like microstructures to the surface of a flexible substrate can decrease static drag and increase swimming speed, and the denticles can be rearranged (into a staggered-overlapping pattern) to further enhance swimming performance (Wen et al., 2014, 2015). Conversely, the external shapes of 3D-printed boxfishes were shown to increase drag, but enhance maneuverability via destabilizing moments induced by the boxy shape; the instabilities facilitate tighter turning (Van Wassenbergh et al., 2015). The microstructure of the boxfish carapace, specifically the suture pattern that connects adjacent scutes, was also shown to increase body rigidity by approximately three times that over a 3D-printed proxy without a hard 'carapace' armor (Kenneson, 2016). Similarly, the square prism structure of a seahorse tail (as compared to a hypothetical cylindrical structure) was shown not only to enhance its resistance to crushing, but also provide several mechanical mechanisms conducive to grasping (Porter et al., 2015).

3D-printing is a powerful tool to build both idealized natural and hypothetical models of fish armors (or other biological systems) – *idealized* because their shapes and structures are representative of the average forms of the armors observed in nature, and *hypothetical* because their shapes and structures are modified to study bioinspired morphologies which do not occur in nature. Such models are excellent proxies for mechanical studies on biological systems, due to their often simplified features that easily reduce the natural complexity of their biological counterparts. Additionally, the stand-in roles of such biomi-

metic systems eliminate the need for destructive mechanical testing on the natural systems they mimic, which are often protected, can have restricted access, or may not be representative of an entire species. This approach allows for comparative analyses of the individual mechanisms that enable the distinct mechanical functions of different armored fishes and other similar natural biological structures.

Acknowledgements

This work was partially supported by the College of Engineering and Science, TIGER Grant, and the Department of Mechanical Engineering, Clemson University (M.M.P. & N.R.), as well as a team Grant from the Fonds de recherche du Québec – Nature et technologies (F.B. & R.M.).

References

Allison, P.G., Chandler, M.Q., Rodriguez, R., Williams, B., Moser, R., Weiss, C., Poda, A., Lafferty, B., Kennedy, A., Seiter, J., 2013. Mechanical properties and structure of the biological multilayered material system, Atractosteus spatula scales. Acta Biomater. 9, 5289–5296.

Araya, S., Zolotovsky, K., Veliz, F., Song, J., Reichert, S., Boyce, M., Ortiz, C., 2013. Bioinformed performative composite structures: from biological micro-structures to material composites and articulated assemblies, computation and performance. In: Proceedings of the 31st International Conference on Education and Research in Computer Aided Architectural Design Delft, The Netherlands.

Barrett, R.D., Rogers, S.M., Schluter, D., 2008. Natural selection on a major armor gene in threespine stickleback. Science 322, 255–257.

Barthelat, F., 2015. Architectured materials in engineering and biology: fabrication, structure, mechanics and performance. Int. Mater. Rev. 60, 413–430.

Barthelat, F., Mirkhalaf, M., 2013. The quest for stiff, strong and tough hybrid materials: an exhaustive exploration. J. R. Soc. Interface 10, 20130711.

Bartol, I.K., Gharib, M., Webb, P.W., Weihs, D., Gordon, M.S., 2005. Body-induced vortical flows: a common mechanism for self-corrective trimming control in boxfishes. J. Exp. Biol. 208, 327–344.

Bartol, I.K., Gordon, M.S., Gharib, M., Hove, J.R., Webb, P.W., Weihs, D., 2002. Flow patterns around the carapaces of rigid-bodied, multi-propulsor boxfishes (Teleostei: ostraciidae). Integr. Comp. Biol. 42, 971–980.

Bartol, I.K., Gharib, M., Weihs, D., Webb, P.W., Hove, J.R., Gordon, M.S., 2003. Hydrodynamic stability of swimming in ostraciid fishes: role of the carapace in the smooth trunkfish Lactophrys triqueter (Teleostei: ostraciidae). J. Exp. Biol. 206, 725–744.

Bauer, J., Schroer, A., Schwaiger, R., Kraft, O., 2016. Approaching theoretical strength in glassy carbon nanolattices. Nat. Mater. 15, 438–443.

Bechert, D., Hoppe, G., Reif, W.-E., 1985. On the drag reduction of the shark skin, AIAA Shear Flow Control Conference.

Bechert, W.D., Bruse, M., Hage, W., Meyer, R., 2000. Fluid mechanics of biological surfaces and their technological application. Naturwissenschaften 87, 157–171.

Besseau, L., Bouligand, Y., 1998. The twisted collagen network of the box-fish scutes. Tissue Cell 30, 251–260.

Bixler, G.D., Bhushan, B., 2012. Biofouling: lessons from nature. Philos. Trans. R. Soc. Lond. A: Math. Phys. Eng. Sci. 370, 2381–2417.

Bouville, F., Maire, E., Meille, S., Van de Moortèle, B., Stevenson, A.J., Deville, S., 2014. Strong, tough and stiff bioinspired ceramics from brittle constituents. Nat. Mater. 13, 508–514.

Browning, A., Ortiz, C., Boyce, M.C., 2013. Mechanics of composite elasmoid fish scale assemblies and their bioinspired analogues. J. Mech. Behav. Biomed. Mater. 19, 75–86.

Bruet, B.J., Song, J., Boyce, M.C., Ortiz, C., 2008. Materials design principles of ancient fish armour. Nat. Mater. 7, 748–756.

Chen, I.H., Kiang, J.H., Correa, V., Lopez, M.I., Chen, P.-Y., McKittrick, J., Meyers, M.A., 2011. Armadillo armor: mechanical testing and micro-structural evaluation. J. Mech. Behav. Biomed. Mater. 4, 713–722.

Chen, P.-Y., Schirer, J., Simpson, A., Nay, R., Lin, Y.-S., Yang, W., Lopez, M.I., Li, J., Olevsky, E.A., Meyers, M.A., 2012. Predation versus protection: fish teeth and scales evaluated by nanoindentation. J. Mater. Res. 27, 100–112.

Chintapalli, R.K., Mirkhalaf, M., Dastjerdi, A.K., Barthelat, F., 2014. Fabrication, testing and modeling of a new flexible armor inspired from natural fish scales and osteoderms. Bioinspiration Biomimetics 9, 036005.

Crofts, S., Summers, A., 2014. How to best smash a snail: the effect of tooth shape on crushing load. J. R. Soc. Interface 11, 20131053.

Dastjerdi, A.K., Barthelat, F., 2015. Teleost fish scales amongst the toughest collagenous materials. J. Mech. Behav. Biomed. Mater. 52, 95–107.

Dean, B., Bhushan, B., 2010. Shark-skin surfaces for fluid-drag reduction in turbulent flow: a review. Philos. Trans. R. Soc. Lond. A: Math. Phys. Eng. Sci. 368, 4775–4806.

Dimas, L.S., Bratzel, G.H., Eylon, I., Buehler, M.J., 2013. Tough composites inspired by mineralized natural materials: computation, 3D printing, and testing. Adv. Funct. Mater. 23, 4629–4638.

Duro-Royo, J., Zolotovsky, K., Mogas-Soldevila, L., Varshney, S., Oxman, N., Boyce, M.C., Ortiz, C., 2015. MetaMesh: a hierarchical computational model for design and fabrication of biomimetic armored surfaces. Comput. – Aided Des. 60, 14–27.

Dyskin, A.V., Estrin, Y., Kanel-Belov, A.J., Pasternak, E., 2003. Topological interlocking of platonic solids: a way to new materials and structures. Philos. Mag. Lett. 83, 197–203.

Ebenstein, D., Calderon, C., Troncoso, O.P., Torres, F.G., 2015. Characterization of dermal plates from armored catfish Pterygoplichthys pardalis reveals sandwich-like nanocomposite structure. J. Mech. Behav. Biomed. Mater. 45, 175–182.

Ehrlich, H., 2015. Biological Materials of Marine Origin: Vertebrates. Springer.

Emily, R., Geoffrey, S., 2009. Bioinspiration—the solution for biofouling control? Bioinspiration Biomimetics 4, 015007.

Espinosa, H.D., Rim, J.E., Barthelat, F., Buehler, M.J., 2009. Merger of structure and material in nacre and bone–Perspectives on de novo biomimetic materials. Progress. Mater. Sci. 54, 1059–1100.

Fischer, J., Wegener, M., 2011. Three-dimensional direct laser writing inspired by stimulated-emission-depletion microscopy. Opt. Mater. Express 1, 614–624.

Fletcher, T., Altringham, J., Peakall, J., Wignall, P., Dorrell, R., 2014. Hydrodynamics of fossil fishes. Proc. R. Soc. Lond. B: Biol. Sci. 281, 20140703.

Fratzl, P., Kolednik, O., Fischer, F.D., Dean, M.N., 2016. The mechanics of tessellations–bioinspired strategies for fracture resistance. Chem. Soc. Rev. 45, 252–267.

Funk, N., Vera, M., Szewciw, L.J., Barthelat, F., Stoykovich, M.P., Vernerey, F.J., 2015. Bioinspired fabrication and characterization of a synthetic fish skin for the protection of soft materials. ACS Appl. Mater. Interfaces 7, 5972–5983.

Gao, W., Zhang, Y., Ramanujan, D., Ramani, K., Chen, Y., Williams, C.B., Wang, C.C., Shin, Y.C., Zhang, S., Zavattieri, P.D., 2015. The status, challenges, and future of additive manufacturing in engineering. Comput. – Aided Des. 69, 65–89.

Garrano, A.M.C., La Rosa, G., Zhang, D., Niu, L.-N., Tay, F., Majd, H., Arola, D., 2012. On the mechanical behavior of scales from Cyprinus carpio. J. Mech. Behav. Biomed. Mater. 7, 17–29.

Gemballa, S., Bartsch, P., 2002. Architecture of the integument in lower teleostomes: functional morphology and evolutionary implications. J. Morphol. 253, 290–309.

Germann, D.P., Schatz, W., Hotz, P.E., 2014. Artificially evolved functional shell morphology of burrowing bivalves. Palaeontol. Electron. 17, 1–25.

Ghosh, R., Ebrahimi, H., Vaziri, A., 2014. Contact kinematics of biomimetic scales. Appl. Phys. Lett. 105, 233701.

Ghosh, R., Ebrahimi, H., Vaziri, A., 2015. Frictional Effects in Biomimetic Scales Engagement. arXiv:1508.03099.

Gil-Duran, S., Arola, D., Ossa, E., 2016. Effect of chemical composition and microstructure on the mechanical behavior of fish scales from Megalops Atlanticus. J. Mech. Behav. Biomed. Mater. 56, 134–145.

Grunenfelder, L., Suksangpanya, N., Salinas, C., Milliron, G., Yaraghi, N., Herrera, S., Evans-Lutterodt, K., Nutt, S., Zavattieri, P., Kisailus, D., 2014. Bio-inspired impact-resistant composites. Acta Biomater. 10, 3997–4008.

Gu, G., Su, I., Sharma, S., Voros, J., Qin, Z., Buehler, M.J., 2016. 3D-printing of bio-inspired composites. J. Biomech. Eng..

Hale, M.E., 1996. Functional morphology of ventral tail bending and prehensile abilities of the seahorse, Hippocampus kuda. J. Morphol. 227, 51–65.

Hebrank, M.R., 1980. Mechanical properties and locomotor functions of eel skin. Biol. Bull. 158, 58–68.

Hebrank, M.R., Hebrank, J.H., 1986. The mechanics of fish skin: lack of an" external tendon" role in two teleosts. Biol. Bull. 171, 236–247.

Huang, Y., Leu, M.C., Mazumder, J., Donmez, A., 2015. Additive manufacturing: current state, future potential, gaps and needs, and recommendations. J. Manuf. Sci. Eng. 137, 014001.

Hubbard, R.P., Melvin, J.W., Barodawala, I.T., 1971. Flexure of cranial sutures. J. Biomech. 4, 491IN1493–1492IN3496.

Ijspeert, A.J., 2014. Biorobotics: using robots to emulate and investigate agile locomotion. Science 346, 196–203.

Ikoma, T., Kobayashi, H., Tanaka, J., Walsh, D., Mann, S., 2003. Microstructure, mechanical, and biomimetic properties of fish scales from Pagrus major. J. Struct. Biol. 142, 327–333.

Jaslow, C.R., 1990. Mechanical properties of cranial sutures. J. Biomech. 23, 313–321.

Jones, F.C., Grabherr, M.G., Chan, Y.F., Russell, P., Mauceli, E., Johnson, J., Swofford, R., Pirun, M., Zody, M.C., White, S., 2012. The genomic basis of adaptive evolution in threespine sticklebacks. Nature 484, 55–61.

Katzschmann, R.K., Marchese, A.D., Rus, D., 2016. Hydraulic Autonomous Soft Robotic Fish for 3D Swimming, Experimental Robotics. Springer, 405–420.

Kenneson, P., 2016. Bioinspired Flexible Armor: the Influence of Suture Interfaces on Tessellated Armor Plates in Bending (B.S. Honors Thesis). Department of Mechanical Engineering. Clemson University.

Kesel, A., Liedert, R., 2007. Learning from nature: non-toxic biofouling control by shark skin effect. Comp. Biochem. Physiol. Part A: Mol. Integr. Physiol. 146, S130.

Khandelwal, S., Siegmund, T., Cipra, R.J., Bolton, J.S., 2012. Transverse loading of cellular topologically interlocked materials. Int. J. Solids Struct. 49, 2394–2403.

Kim, S., Su, Y., Mihi, A., Lee, S., Liu, Z., Bhandakkar, T.K., Wu, J., Geddes, J.B., Johnson, H.T., Zhang, Y., 2012. Imbricate scales as a design construct for microsystem technologies. Small 8, 901–906.

Kirschner, C.M., Brennan, A.B., 2012. Bio-inspired antifouling strategies. In: Clarke, D.R. (Ed.), Annual Review of Materials Research 42. Annual Reviews, Palo Alto, 211–229.

Kokkinis, D., Schaffner, M., Studart, A.R., 2015. Multimaterial magnetically assisted 3D printing of composite materials. Nat. Commun. 6.

Kuusipalo, L., 1998. Scale morphology in Malawian cichlids. J. Fish. Biol. 52, 771–781.

Lang, A.W., Motta, P., Hidalgo, P., Westcott, M., 2008. Bristled shark skin: a microgeometry for boundary layer control? Bioinspiration Biomimetics 3, 046005.

Lauder, G.V., 2015. Fish locomotion: recent advances and new directions. Annu. Rev. Mar. Sci. 7, 521–545.

Le Ferrand, H., Bouville, F., Niebel, T.P., Studart, A.R., 2015. Magnetically assisted slip

casting of bioinspired heterogeneous composites. Nat. Mater. 14, 1172–1179.
Levangie, P.K., Norkin, C.C., 2011. Joint Structure and Function: A Comprehensive Analysis. FA Davis.
Li, L., Ortiz, C., 2015. A natural 3D interconnected laminated composite with enhanced damage resistance. Adv. Funct. Mater. 25, 3463–3471.
Li, Y., Ortiz, C., Boyce, M.C., 2011. Stiffness and strength of suture joints in nature. Phys. Rev. E 84, 062904.
Li, Y., Ortiz, C., Boyce, M.C., 2012. Bioinspired, mechanical, deterministic fractal model for hierarchical suture joints. Phys. Rev. E 85, 031901.
Li, Y., Ortiz, C., Boyce, M.C., 2013. A generalized mechanical model for suture interfaces of arbitrary geometry. J. Mech. Phys. Solids 61, 1144–1167.
Lin, E., Li, Y., Ortiz, C., Boyce, M.C., 2014a. 3D printed, bio-inspired prototypes and analytical models for structured suture interfaces with geometrically-tuned deformation and failure behavior. J. Mech. Phys. Solids 73, 166–182.
Lin, E., Li, Y., Weaver, J.C., Ortiz, C., Boyce, M.C., 2014b. Tunability and enhancement of mechanical behavior with additively manufactured bio-inspired hierarchical suture interfaces. J. Mater. Res. 29, 1867–1875.
Lin, Y., Wei, C., Olevsky, E., Meyers, M.A., 2011. Mechanical properties and the laminate structure of Arapaima gigas scales. J. Mech. Behav. Biomed. Mater. 4, 1145–1156.
Lippitsch, E., 1990. Scale morphology and squamation patterns in cichlids (Teleostei, Perciformes): a comparative study. J. Fish. Biol. 37, 265–291.
Liu, K.S., Jiang, L., 2012. Bio-inspired self-cleaning surfaces. In: Clarke, D.R. (Ed.), Annual Review of Materials Research 42. Annual Reviews, Palo Alto, 231–263.
Long, J., Hale, M., Mchenry, M., Westneat, M., 1996. Functions of fish skin: flexural stiffness and steady swimming of longnose gar, Lepisosteus osseus. J. Exp. Biol. 199, 2139–2151.
Marcroft, T.A., 2015. Evolution of the Boxfish Carapace: Functional Consequences of Shape (M.S. Thesis). Department of Biology. University of California, Los Angeles.
Martin, J.J., Fiore, B.E., Erb, R.M., 2015. Designing bioinspired composite reinforcement architectures via 3D magnetic printing. Nat. Commun. 6.
Martini, R., Barthelat, F., 2016. Stability of hard plates on soft substrates and application to the design of bioinspired segmented armor. J. Mech. Phys. Solids..
McInroe, B., Astley, H.C., Gong, C., Kawano, S.M., Schiebel, P.E., Rieser, J.M., Choset, H., Blob, R.W., Goldman, D.I., 2016. Tail use improves performance on soft substrates in models of early vertebrate land locomotors. Science 353, 154–158.
Meng, J., Zhang, P., Wang, S., 2016. Recent progress of abrasion-resistant materials: learning from nature. Chem. Soc. Rev. 45, 237–251.
Meyers, M.A., McKittrick, J., Chen, P.-Y., 2013. Structural biological materials: critical mechanics-materials connections. Science 339, 773–779.
Meyers, M.A., Lin, Y., Olevsky, E., Chen, P.Y., 2012. Battle in the Amazon: arapaima versus piranha. Adv. Eng. Mater. 14, B279–B288.
Mirkhalaf, M., Dastjerdi, A.K., Barthelat, F., 2014. Overcoming the brittleness of glass through bio-inspiration and micro-architecture. Nat. Commun. 5.
Mirkhalaf, M., Tanguay, J., Barthelat, F., 2016. Carving 3D architectures within glass: exploring new strategies to transform the mechanics and performance of materials. Extrem. Mech. Lett..
Mirzaeifar, R., Dimas, L.S., Qin, Z., Buehler, M.J., 2015. Defect-tolerant bioinspired hierarchical composites: simulation and experiment. ACS Biomater. Sci. Eng. 1, 295–304.
Mohammed, J.S., 2016. Applications of 3D printing technologies in oceanography. Methods Oceanogr. 17, 97–117.
Molotnikov, A., Gerbrand, R., Qi, Y., Simon, G., Estrin, Y., 2015. Design of responsive materials using topologically interlocked elements. Smart Mater. Struct. 24, 025034.
Motta, P., Habegger, M.L., Lang, A., Hueter, R., Davis, J., 2012. Scale morphology and flexibility in the shortfin mako Isurus oxyrinchus and the blacktip shark Carcharhinus limbatus. J. Morphol. 273, 1096–1110.
Murphy, S.V., Atala, A., 2014. 3D bioprinting of tissues and organs. Nat. Biotechnol. 32, 773–785.
Naleway, S.E., Porter, M.M., McKittrick, J., Meyers, M.A., 2015. Structural design elements in biological materials: application to bioinspiration. Adv. Mater. 27, 5455–5476.
Nelson, J.S., 2006. Fishes of the World. John Wiley & Sons.
Neutens, C., Adriaens, D., Christiaens, J., De Kegel, B., Dierick, M., Boistel, R., Van Hoorebeke, L., 2014. Grasping convergent evolution in syngnathids: a unique tale of tails. J. Anat. 224, 710–723.
Nishimoto, S., Bhushan, B., 2013. Bioinspired self-cleaning surfaces with superhydrophobicity, superoleophobicity, and superhydrophilicity. RSC Adv. 3, 671–690.
de Obaldia, E.E., Jeong, C., Grunenfelder, L.K., Kisailus, D., Zavattieri, P., 2015. Analysis of the mechanical response of biomimetic materials with highly oriented microstructures through 3D printing, mechanical testing and modeling. J. Mech. Behav. Biomed. Mater. 48, 70–85.
Oeffner, J., Lauder, G.V., 2012. The hydrodynamic function of shark skin and two biomimetic applications. J. Exp. Biol. 215, 785–795.
Porter, M.M., Novitskaya, E., Castro-Ceseña, A.B., Meyers, M.A., McKittrick, J., 2013. Highly deformable bones: unusual deformation mechanisms of seahorse armor. Acta Biomater. 9, 6763–6770.
Porter, M.M., Adriaens, D., Hatton, R.L., Meyers, M.A., McKittrick, J., 2015. Why the seahorse tail is square. Science 349, aaa6683.
Praet, T., Adriaens, D., Cauter, S.V., Masschaele, B., Beule, M.D., Verhegghe, B., 2012. Inspiration from nature: dynamic modelling of the musculoskeletal structure of the seahorse tail. Int. J. Numer. Methods Biomed. Eng. 28, 1028–1042.
Qin, Z., Dimas, L., Adler, D., Bratzel, G., Buehler, M.J., 2014. Biological materials by design. J. Phys.: Condens. Matter 26, 073101.
Raj, A., Thakur, A., 2016. Fish-inspired robots: design, sensing, actuation, and autonomy—a review of research. Bioinspiration Biomimetics 11, 031001.
Rankouhi, B., Javadpour, S., Delfanian, F., Letcher, T., 2016. Failure analysis and mechanical characterization of 3D printed ABS with respect to layer thickness and orientation. J. Fail. Anal. Prev. 16, 467–481.
Raschi, W., Tabit, C., 1992. Functional aspects of Placoid Scales: a review and update. Mar. Freshw. Res. 43, 123–147.
Reza, E.H., Somayeh, B., Halimeh, Z., Fatemeh, S., 2009. Scale morphology of tank goby Glossogobius giuris (Hamilton-Buchanan, 1822) (Perciformes: gobiidae) using scanning electron microscope. J. Biol. Sci. 9, 899–903.
Ritchie, R.O., 2011. The conflicts between strength and toughness. Nat. Mater. 10, 817–822.
Rudykh, S., Boyce, M.C., 2014a. Analysis of elasmoid fish imbricated layered scale-tissue systems and their bio-inspired analogues at finite strains and bending. IMA J. Appl. Math. 79, 830–847.
Rudykh, S., Boyce, M.C., 2014b. Transforming small localized loading into large rotational motion in soft anisotropically structured materials. Adv. Eng. Mater. 16, 1311–1317.
Rudykh, S., Ortiz, C., Boyce, M.C., 2015. Flexibility and protection by design: imbricated hybrid microstructures of bio-inspired armor. Soft Matter 11, 2547–2554.
Schubert, C., van Langeveld, M.C., Donoso, L.A., 2013. Innovations in 3D printing: a 3D overview from optics to organs. Br. J. Ophthalmol., [bjophthalmol-2013-304446].
Sen, D., Buehler, M.J., 2011. Structural hierarchies define toughness and defect-tolerance despite simple and mechanically inferior brittle building blocks. Sci. Rep. 1.
Sharklet Technologies, Inc., 2007. ⟨www.sharklet.com⟩, (accessed 10.12.16).
Shephard, K.L., 1994. Functions for fish mucus. Rev. Fish. Biol. Fish. 4, 401–429.
Sire, J.Y., 1993. Development and fine structure of the bony scutes in Corydoras arcuatus (Siluriformes, Callichthyidae). J. Morphol. 215, 225–244.
Sire, J.Y., Donoghue, P.C., Vickaryous, M.K., 2009. Origin and evolution of the integumentary skeleton in non-tetrapod vertebrates. J. Anat. 214, 409–440.
Sire, J.-Y., 1989. From ganoid to elasmoid scales in the Actinopterygian fishes. Neth. J. Zool. 40, 75–92.
Sire, J.-Y., Huysseune, A., 2003. Formation of dermal skeletal and dental tissues in fish: a comparative and evolutionary approach. Biol. Rev. 78, 219–249.
Song, J., Ortiz, C., Boyce, M.C., 2011. Threat-protection mechanics of an armored fish. J. Mech. Behav. Biomed. Mater. 4, 699–712.
Song, J., Reichert, S., Kallai, I., Gazit, D., Wund, M., Boyce, M.C., Ortiz, C., 2010. Quantitative microstructural studies of the armor of the marine threespine stickleback (Gasterosteus aculeatus). J. Struct. Biol. 171, 318–331.
Studart, A.R., 2016. Additive manufacturing of biologically-inspired materials. Chem. Soc. Rev. 45, 359–376.
Studart, A.R., Erb, R.M., Libanori, R., 2015. Bioinspired Hierarchical Composites, Hybrid and Hierarchical Composite Materials. Springer, 287–318.
Sudo, S., Tsuyuki, K., Ito, Y., Ikohagi, T., 2002. A study on the surface shape of fish scales. JSME Int. J. Ser. C Mech. Syst. Mach. Elem. Manuf. 45, 1100–1105.
Tiwary, C.S., Kishore, S., Sarkar, S., Mahapatra, D.R., Ajayan, P.M., Chattopadhyay, K., 2015. Morphogenesis and mechanostabilization of complex natural and 3D printed shapes. Sci. Adv. 1, e1400052.
Torres, F., Malásquez, M., Troncoso, O., 2015. Impact and fracture analysis of fish scales from Arapaima gigas. Mater. Sci. Eng.: C 51, 153–157.
Vaezi, M., Seitz, H., Yang, S., 2013. A review on 3D micro-additive manufacturing technologies. Int. J. Adv. Manuf. Technol. 67, 1721–1754.
Valashani, S.M.M., Barthelat, F., 2015. A laser-engraved glass duplicating the structure, mechanics and performance of natural nacre. Bioinspiration Biomimetics 10, 026005.
Van Wassenbergh, S., van Manen, K., Marcroft, T.A., Alfaro, M.E., Stamhuis, E.J., 2015. Boxfish swimming paradox resolved: forces by the flow of water around the body promote manoeuvrability. J. R. Soc. Interface 12, 20141146.
Varshney, S., Song, J., Li, Y., Boyce, M.C., Ortiz, C., 2015. Morphometric structural diversity of a natural armor assembly investigated by 2D continuum strain analysis. J. Struct. Biol. 192, 487–499.
Vernerey, F.J., Barthelat, F., 2010. On the mechanics of fishscale structures. Int. J. Solids Struct. 47, 2268–2275.
Vernerey, F.J., Barthelat, F., 2014. Skin and scales of teleost fish: simple structure but high performance and multiple functions. J. Mech. Phys. Solids 68, 66–76.
Vernerey, F.J., Musiket, K., Barthelat, F., 2014. Mechanics of fish skin: a computational approach for bio-inspired flexible composites. Int. J. Solids Struct. 51, 274–283.
Vickaryous, M.K., Hall, B.K., 2006. Osteoderm morphology and development in the nine-banded armadillo, Dasypus novemcinctus (Mammalia, Xenarthra, Cingulata). J. Morphol. 267, 1273–1283.
Vickaryous, M.K., Sire, J.Y., 2009. The integumentary skeleton of tetrapods: origin, evolution, and development. J. Anat. 214, 441–464.
Waghmare, P.R., Gunda, N.S.K., Mitra, S.K., 2014. Under-water superoleophobicity of fish scales. Sci. Rep. 4.
Wainwright, S.A., Vosburgh, F., Hebrank, J.H., 1978. Shark skin: function in locomotion. Science 202, 747–749.
Walker, J.A., 2000. Does a rigid body limit maneuverability? J. Exp. Biol. 203, 3391–3396.
Wang, L., Song, J., Ortiz, C., Boyce, M.C., 2009. Anisotropic design of a multilayered biological exoskeleton. J. Mater. Res. 24, 3477.
Wang, R., Gupta, H.S., 2011. Deformation and fracture mechanisms of bone and nacre. Annu. Rev. Mater. Res. 41, 41–73.
Webb, P.W., Hardy, D.H., Mehl, V.L., 1992. The effect of armored skin on the swimming of longnose gar. Lepisosteus Osseus. Can. J. Zool. 70, 1173–1179.
Wegst, U., Ashby, M., 2004. The mechanical efficiency of natural materials. Philos. Mag. 84, 2167–2186.
Wegst, U.G., Bai, H., Saiz, E., Tomsia, A.P., Ritchie, R.O., 2015. Bioinspired structural

materials. Nat. Mater. 14, 23–36.
Wen, L., Weaver, J.C., Lauder, G.V., 2014. Biomimetic shark skin: design, fabrication and hydrodynamic function. J. Exp. Biol. 217, 1656–1666.
Wen, L., Weaver, J.C., Thornycroft, P.J., Lauder, G.V., 2015. Hydrodynamic function of biomimetic shark skin: effect of denticle pattern and spacing. Bioinspiration Biomimetics 10, 066010.
Wong, K.V., Hernandez, A., 2012. A review of additive manufacturing. ISRN Mech. Eng. 2012.
Wu, W., Geng, P., Li, G., Zhao, D., Zhang, H., Zhao, J., 2015. Influence of layer thickness and raster angle on the mechanical properties of 3D-printed PEEK and a comparative mechanical study between PEEK and ABS. Materials 8, 5834–5846.
Yang, W., Naleway, S.E., Porter, M.M., Meyers, M.A., McKittrick, J., 2015. The armored carapace of the boxfish. Acta Biomater. 23, 1–10.
Yang, W., Chen, I.H., Gludovatz, B., Zimmermann, E.A., Ritchie, R.O., Meyers, M.A., 2013a. Natural flexible dermal armor. Adv. Mater. 25, 31–48.
Yang, W., Gludovatz, B., Zimmermann, E.A., Bale, H.A., Ritchie, R.O., Meyers, M.A., 2013b. Structure and fracture resistance of alligator gar (Atractosteus spatula) armored fish scales. Acta Biomater. 9, 5876–5889.
Yang, W., Sherman, V.R., Gludovatz, B., Mackey, M., Zimmermann, E.A., Chang, E.H., Schaible, E., Qin, Z., Buehler, M.J., Ritchie, R.O., 2014. Protective role of Arapaima gigas fish scales: structure and mechanical behavior. Acta Biomater. 10, 3599–3614.
Zhu, D., Szewciw, L., Vernerey, F., Barthelat, F., 2013. Puncture resistance of the scaled skin from striped bass: collective mechanisms and inspiration for new flexible armor designs. J. Mech. Behav. Biomed. Mater. 24, 30–40.
Zhu, D., Ortega, C.F., Motamedi, R., Szewciw, L., Vernerey, F., Barthelat, F., 2012. Structure and mechanical performance of a “modern” fish scale. Adv. Eng. Mater. 14, B185–B194.
Zimmermann, E.A., Gludovatz, B., Schaible, E., Dave, N.K., Yang, W., Meyers, M.A., Ritchie, R.O., 2013. Mechanical adaptability of the Bouligand-type structure in natural dermal armour. Nat. Commun. 4.
Zylberberg, L., Meunier, F., 1981. Evidence of denticles and attachment fibres in the superficial layer of scales in two fishes: Carassius auratus and Cyprinus carpio (Cyprinidae, Teleostei). J. Zool. 195, 459–471.